Journal of Traditional and Complementary Medicine 14 (2024) 477–493

Contents lists available at ScienceDirect

Journal of Traditional and Complementary Medicine

journal homepage: www.elsevier.com/locate/jtcme

Chemical profiling and mechanisms of Agarikon pill in a rat model of cigarette smoke-induced chronic obstructive pulmonary disease

Aizaiti Keremu [a,b], Zulfiye Talat [c], Xueying Lu [a], Rahima Abdulla [b], Maidina Habasi [a], Haji Akber Aisa [a,b,*]

[a] State Key Laboratory Basis of Xinjiang Indigenous Medicinal Plants Resource Utilization, Xinjiang Technical Institute of Physics and Chemistry, Chinese Academy of Sciences, Urumqi, 830011, China
[b] University of Chinese Academy of Sciences, Beijing, 100049, China
[c] Prescription Laboratory of Xinjiang Traditional Uyghur Medicine, Xinjiang Institute of Traditional Uyghur Medicine, Urumqi, China

ARTICLE INFO

Keywords:
Chronic obstructive pulmonary disease (COPD)
Agarikon pill
Traditional Chinese medicine
Inflammatory response
Network pharmacology

ABSTRACT

Background and aim: Agarikon pill (AGKP), a traditional Chinese herbal formula, and has been used for chronic obstructive pulmonary disease (COPD) treatment clinically. However, the active components and exact pharmacological mechanisms are still unclear. We aimed to investigate the therapeutic effects and mechanisms of AGKP on COPD and identify the chemical constituents and active compounds.

Experimental procedure: The chemical components of AGKP were identified by ultrahigh-performance liquid chromatography coupled with quadrupole/orbitrap high-resolution mass spectrometry (UHPLC-Q-Orbitrap-HRMS). Network pharmacology analysis was performed to uncover the potential mechanism of AGKP. The efficiencies and mechanisms of AGKP were further confirmed in COPD animal models.

Results and conclusion: Ninety compounds from AGKP, such as flavonoids, triterpenoids, saponins, anthracenes, derivatives, phenyl propionic acid, and other organic acids, were identified in our study. AGKP improved lung function and pathological changes in COPD model rats. Additionally, inflammatory cell infiltration and proinflammatory cytokine levels were markedly reduced in COPD rats administered AGKP. Network pharmacology analysis showed that the inflammatory response is the crucial mechanism by which AGKP exerts therapeutic effects on COPD rats. WB and PCR data indicated that AGKP attenuated the inflammatory response in COPD model rats. AGKP reduces the pulmonary inflammatory response through the PI3K/AKT and MAPK TLR/NF-κB signaling pathways and exerts therapeutic effects via inhibition of inflammation and mucus hypersecretion on COPD model rats.

1. Introduction

Chronic obstructive pulmonary disease (COPD) is one of the top three killers with high morbidity and mortality worldwide.[1] As a chronic multifactorial inflammatory lung disease, COPD is mainly characterized by reversible airflow obstruction and systemic inflammation.[2] At present, although some treatments are effective in prohibiting the progression of COPD, reducing airway obstruction and enhancing the quality of life of COPD patients, the results are not desirable.[3] Therefore, exploring effective and safe therapies for COPD has become a pressing issue due to the complexity and refractory nature of COPD. Recently, traditional Chinese medicine (TCM) for the treatment of COPD has been widely studied, and has better efficiency, high safety and low cost.[4,5]

Nuclear factor κB (NF-κB), mitogen-activated protein kinases (MAPKs) and Toll-like receptor (TLR) 4/2 are the major pathways that play important roles in airway inflammation in COPD.[6,7] Abnormal activation of these pathways can induce lung tissue damage and reduce lung function by upregulating the expression of various inflammatory genes and promoting the release of pro-inflammatory cytokines, such as

Peer review under responsibility of The Center for Food and Biomolecules, National Taiwan University.

* Corresponding author. State Key Laboratory Basis of Xinjiang Indigenous Medicinal Plants Resource Utilization, CAS Key Laboratory of Chemistry of Plant Resources in Arid Regions, Xinjiang Technical Institute of Physics and Chemistry, Chinese Academy of Sciences, Beijing South Road 40-1, Urumqi, 830011, Xinjiang, China.

E-mail addresses: ezzatgul0993@163.com (A. Keremu), zulfiyetalat@163.com (Z. Talat), xueyinglu@ms.xjb.ac.cn (X. Lu), rahima@ms.xjb.ac.cn (R. Abdulla), maidn@ms.xjb.ac.cn (M. Habasi), aisa@ms.xjb.ac.cn (H.A. Aisa).

https://doi.org/10.1016/j.jtcme.2024.03.006
Received 24 August 2023; Received in revised form 6 January 2024; Accepted 5 March 2024
Available online 6 March 2024

List of abbreviations

AGKP	Agarikon Pill
COPD	Chronic obstructive pulmonary disease
UHPLC-Q-Orbitrap-HRMS	Ultrahigh-performance liquid chromatography coupled with quadrupole/orbitrap high-resolution mass spectrometry
CS	Cigarette smoke
LPS	Lipopolysaccharide
Mont	Montelukast
GK	Guilong Kechuanning capsules
IL	Interleukin
TNF-α	Tumor necrosis factor α
TGF-β	Transforming growth factor beta
EF50%	Expiratory flow at 50% tidal volume
TV	Tidal volume
PIF	Peak inspiratory flow
PEF	Peak expiratory flow
ELISA	enzyme-linked immunosorbent assay
PCR	Polymerase chain reaction
EGFR	Epidermal growth factor receptor
PI3K	Phosphatidylinositol 3-kinase
MUC5AC	Mucin 5AC
MUC5B	Mucin 5B
MAPK	Mitogen-activated protein kinase
JNK	Jun N-terminal kinase
ERK	Extracellular signal-regulated kinase
NF-κB	Nuclear factor-κB
TLRs	Toll-like receptors

TNF-α, IL-1β and IL-6, resulting in the promotion of COPD progression.[8,9] Additionally, airway mucus hypersecretion is an important pathophysiological feature of COPD; it is not only a symptom but also an independent risk factor for COPD progression and prognosis.[10] MUC5AC and MUC5B are the most important and abundant mucins, and the level of MUC5AC in airway epithelial cells reflects the intensity of airway mucin secretion; abnormalities in its quantity and quality have a negative impact on airway function.[11] Therefore, anti-inflammatory therapy and inhibition of mucus hypersecretion are the main treatment strategies for COPD.[12–14]

Agarikon pill (AGKP), a clinically experienced formula, was first recorded in the ancient traditional medicinal book *KarabadanKadiri* (in the year 1780), and it has been recorded to "purge the lung, dissolve phlegm, and relieve cough and asthma". As a result of the excellent curative effects of AGKP on improve lung function by expectoration and reducing inflammation patients with COPD for many years, it has been used by local Traditional Chinese Medicine (TCM) hospitals as a hospital prescription.[15] It is the pharmaceutical preparation in medical institutions registered by Uyghur Medical Hospital of Xinjiang Uyghur Autonomous Region of China (approval number is M20041561). AGKP has been also collected in Drug Standard of Ministry of Public Health of the People's Republic of China-Uyghur medicine part. It consists of six crude herbs, including *Glycyrrhiza uralensis* Fisch., *Fomes officinalis* (Vill. ex Fr.) Ames, *Citrullus colocynthis* (L.) Schrad., *Operculina turpethum* (L.) Silva Manso, *Aloe vera* (L.) Burm. f., and *Astragalus sarcocolla* Dymock.[16] Among them, *Fomes officinalis* (Vill. ex Fr.) Ames and *Glycyrrhiza uralensis* Fisch. exert considerable therapeutic effects on COPD, and their active components liquiritin, isoliquiritin, glycyrrhizic acid and 18β-Glycyrrhetinic acid have anti-inflammation effects[17,18] that are related to the pathogenesis of lung inflammation in COPD. However, there is no modern pharmacological research to support its therapeutic effect and mechanism on COPD, which limits its wide clinical application. Thus, it is necessary to explore the chemical composition and mechanism of action of AGKP on COPD.

In this study, we analyzed the chemical compounds of AGKP by UHPLC-Q-Orbitrap-HRMS, and the network pharmacology method was used to predict the molecular mechanism of COPD. Montelukast was used as the positive control drug, and animal experiments on lipopolysaccharide (LPS) and cigarette smoke (CS)-induced COPD model rats were conducted to explore the pharmacological effects of AGKP against COPD. The possible mechanisms of AGKP were confirmed using molecular biology methods based on the results of network pharmacology.

2. Materials and methods

2.1. Reagents and medicinal materials

AGKP is composed of six Chinese herbal medicines, which were purchased from Xinjiang XinLvbao Pharmaceutical Co., Ltd. (Hetian, Xinjiang, China). The ingredients of AGKP are shown in Table 1. The plant names have been proofed with the data in www.Theplantlist.org. The quality of all herbal medicines was identified by Dr. Li Chen, Xinjiang Technical Institute of Physics and Chemistry, Chinese Academy of Sciences. Montelukast (Mont, batch number: T024718) was provided by Merck Sharp Dohme Ltd. (U.K.). Guilong Kechuanning capsules (GK, batch number 150509) were purchased from Guilong Pharmaceutical Co., Ltd. (Anhui, China). Lipopolysaccharide (LPS) was supplied by Sigma Chemical Co., Ltd. (L2880, St. Louis, MO, USA). Liquiritin (1116–201106) and glycyrrhizic acid (110731–202021) were supplied by the China Institute of Food and Drug Control (Beijing, China). Isoliquiritin (P0462), liquiritigenin (P0296), quinic acid (15073002), glabridin (17020903), aloeresin D (20072603), aloe-emodin (19010803), aloin A (21011505), aloin B (20062002), kaempferol (p0013) and isoliquiritigenin (P0039) were purchased from Shanghai Chunyou Biotechnology Co., Ltd. (Shanghai, China). HPLC–MS grade methanol and acetonitrile were supplied by Fisher Scientific (Fair Lawn, NJ, USA). All other reagents and chemicals were analytically pure and purchased from Beijing Chemical Co., Ltd. (Beijing, China).

2.2. Animals

SPF-grade healthy male Sprague–Dawley (SD) rats were provided by the Animal Center of Xinjiang Medical University (Urumqi, China) [weighing 200 ± 20 g; Production license No. SCXK (Xin) 2018-0002;

Table 1
The compositions of Agarikon pill formula.

No.	Chinese name	Latin name	Produced from	Dosage (g)
1	Gancao	*Glycyrrhiza uralensis* Fisch.	Dry root	7.0
2	Alihong	*Fomes officinalis* (Vill. ex Fr.) Ames	Dry fruiting body	10.5
3	Luhui	*Aloe vera* (L.) Burm.f.	Dried matter of leaf fluid	7.0
4	Yaoxigua	*Citrullus colocynthis* (L.) Schrad.	Fruit	7.0
5	Heguoteng	*Operculina turpethum* (L.) Silva Manso.	Dry root	10.5
6	Gancaoweijiao	*Astragalus sarcocolla* Dymock.	Gum resin	7.0

Combined use license No. SYXK (Xin): 2018-0003]. The animal study was approved by the Ethics Committee of Xinjiang Medical University (approval No. IACUC-20210315-17) and were performed in accordance with the Guide for the Care and Use of Laboratory Animals published by the Ministry of Health of China. All efforts were made to minimize animal suffering and reduce the number of animals used. All rats were housed under standardized housing conditions (12/12 h light/dark cycle; temperature, 22 ± 2 °C; relative humidity, 50 ± 5%) and were provided food and water ad libitum.

2.3. UHPLC-Q-orbitrap-HRMS analysis of AGKP samples

The extract was prepared from 5 g of AGKP sample by adding 100 mL methanol and heating under reflux for 1 h. After cooling to room temperature, 1 mL of supernatant was centrifuged at 13000 r/min for 10 min and filtered through a 0.22 μm microporous membrane, which was then used for UHPLC-HRMS analysis.

Chemical component analysis of AGKP was performed on an UHPLC-Q-Orbitrap-HRMS and chromatographic separation on a Waters XBridge C18 column (4.6 × 250 mm, 5 μm). The solvent system consisted of solvent A (0.1% formic acid in water) and solvent B (acetonitrile) with a linear gradient (0 min 5% B, 7 min 5~20% B, 10 min 20~22% B, 13 min 22~25% B, 18 min 25% B, 35 min 25~30% B, 40 min 30~45% B, 50 min 45~80% B, 60 min 80~100% B) at a flow rate of 1.0 mL/min. MS detection was at a scan range of 100–1500 mass-to-charge ratio (m/z) in both the positive and negative ionization modes. The parameters of the electrospray ionization (ESI) source were as follows: heating temperature 300 °C; capillary temperature 350 °C; auxiliary gas flow 10 arb; sheath gas flow 40 arb, voltage 3.5 kV in positive mode; sheath gas flow 38 arb, voltage 2.8 kV in negative mode; stepped normalized collision energy (NCE) 30, 50, or 70; full mass resolution ratio 70,000 (FWHM); dd-MS2 17500 (FWHM). All data acquisition and processing were executed by Xcalibur 4.2 software (Thermo Fisher Scientific Inc., USA).

2.4. Data preparation and target prediction

First, the components obtained from UHPLC-Q-Orbitrap-HRMS analysis were preprocessed and normalized, and finally, the component names were entered into the PubChem database. Three-dimensional molecular structure descriptors were obtained, and then the pharmacokinetic parameters associated with the chemical composition were derived through Swiss Institute of Bioinformatics (SIB), a database in which the bioactive components were further studied based on absorption, distribution, metabolism, and excretion (ADME).[19] High gastrointestinal absorption and bioavailability scores ≥0.55 were used as screening criteria. The final screened components were used as active ingredients in AGKP for the treatment of COPD.

We downloaded the obtained AGKP components' normalized three-dimensional molecular structures or SMILES IDs from the PubMed database (https://www.ncbi.nlm.nih.gov/). The targets of AGKP components were screened using SIB (http://www.swisstargetprediction.ch/). Cytoscape 3.8.2 software (https://cytoscape.org) was used to construct the component-target network. To collect the disease targets for COPD, the TCMIP V2.0 database (http://www.tcmip.cn/TCMIP/index.php), DisGeNET database (http://www.disgenet. org) and GeneCards database (http://www.genecards.org/) were searched using "chronic obstructive pulmonary disease" as the keyword. The Comparative Toxicogenomics Database (CTD) (http://ctdbase.org) was also searched using "Inference score ≥40″ as the keyword to screen the known COPD disease targets.[19] The known COPD targets can be obtained after the duplicate targets have been removed.

2.5. Network construction and analysis

The target intersections between AGKP and COPD were imported into the STRING database (https://string-db.org/) to perform protein–protein interaction (PPI) analysis. The organism was specified as "*Homo sapiens*", the "minimum required interaction score" was selected as ≥ 0.999, and the default parameters were used in other settings. Then, a PPI network was constructed based on the interaction relationship between the targets. Subsequently, to evaluate the therapeutic mechanism of AGKP in treating COPD, the PPI network was inputted into Cytoscape 3.8.2 software using the CytoNCA (2.1.6) plug-in (using "Ranking method: DMNC" as the qualifier) to analyze the topology of the intersection network.[20] The Degree Value were used to sift the top 15 hub targets form the network and finally got the critical targets of AGKP for treating COPD.

GO enrichment analysis and KEGG signal pathway enrichment analysis were performed in the DAVID database (https://david.ncifcrf.gov/) with the screening criteria of "FDR (false discovery rate) ≤ 0.01".[19]

Molecular docking verification was performed on 48 active compounds and 4 important targets in AGKP to investigate potential binding effects between the active ingredients and the targets. In detail, first, the crystal structure of the target protein was retrieved from the Protein Data Bank (PDB) (https://www.rcsb.org). 3D structures of the active ingredients of AGKP were obtained from the PubChem (https://pubchem.ncbi.nlm.nih.gov/). Secondly, the molecular ligands and proteins was changed to pdbqt format by AutoDock Tools after removing the water molecules and organic compounds from ligands and the addition non-polar hydrogen bridge. Third, the receptor protein was subsequently docked with the small molecule ligands of the main compounds using AutoDock Vina (version: 1.2, http://vina.scripps.edu/index.html), and the dominant conformation was taken for analysis and plotted with PyMOL software.[20]

2.6. COPD animal model establishment and AGKP treatment

Prior to the experimental procedure, the rats were acclimatized for one week. The COPD model rats were exposed to CS in a smoking chamber twice a day with a 4-h interval using a standard smoking apparatus, except for days that they were administered LPS. The rats were sensitized on day 1 and day 25 with 0.2 mL of LPS (1 mg/mL) administered to the lung airways. The control rats were exposed to room air, and a normal saline solution with an equivalent volume to LPS was administered. In the experimental period, the body weights of the rats were recorded once a week.[13] The success criteria for the establishment of the COPD model were evaluated according to lung function changes and lung tissue pathology.

After 5 weeks, the rats were randomly divided into seven subgroups: (1) the control group (rats that intragastrically received normal saline); (2) COPD model group (COPD rats that intragastrically received normal saline); (3) COPD with montelukast (Mont) treatment group (COPD rats that intragastrically treated with Mont 1 mg/kg/d); (4) COPD with Guilong Kechuanning capsules (GK) group (COPD rats that intragastrically treated with GK 720 mg/kg/day); (5) COPD with AGKP low-dosage group (COPD rats that intragastrically treated with AGKP 225 mg/kg/day, AGKP-L); (6) COPD with AGKP middle-dosage group (COPD rats that intragastrically treated with AGKP 450 mg/kg/day, AGKP-M); and (7) COPD with high-dosage group (COPD rats that intragastrically treated with AGKP 900 mg/kg/day, AGKP-H), 12 rats in each group. All groups were administered their respective doses by oral gavage once per day for 4 weeks. The body weights of the rats were recorded once a week and 1 h after the last administration, pulmonary function and pulmonary histopathology were observed, and blood, bronchoalveolar lavage fluid (BALF), and lung tissue samples were collected (Fig. 1). All rats were sacrificed by intraperitoneal injection of pentobarbital sodium with 150–200 mg/kg which can produce respiratory arrest, if necessary experimental animal heartbeat was checked.

2.7. Measurement of pulmonary function

At the 4th week of administration, the tidal volume (TV), peak

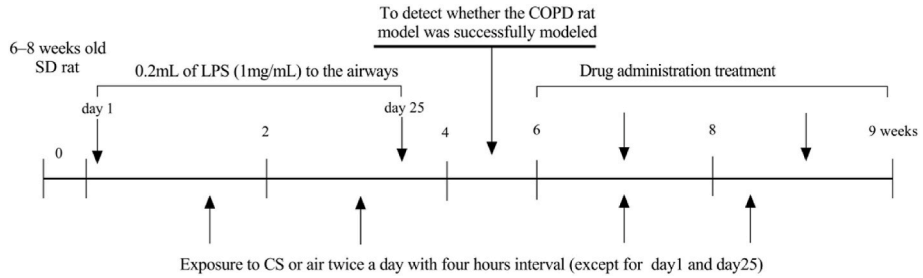

Fig. 1. Flow chart of animal Experiments.

inspiratory flow (PIF), peak expiratory flow (PEF) and expiratory flow at 50% tidal volume (EF50), airway narrowing index (Penh, reflecting respiratory resistance) and PAU (time comparison between early and late expiration) were measured by unlimited pulmonary function plethysmography (Buxco Inc., Wilmington, NC, USA).

2.8. Pulmonary histopathology observation

After sacrifice, the whole middle lobe of the right lung of each animal was fixed overnight with 4% paraformaldehyde at room temperature. The tissues were embedded in paraffin, sectioned, and stained with H&E, and the pathological changes were observed under a light microscope (Leica LAS X, Leica, Germany). Mean linear intercept (MLI) was determined as follow. Following the drawing of a cross (+) through the middle of each image (the visual field that would affect the result are not selected, such as where the guideline intersects with a blood vesse or a bronchus, and where the guideline is partially outside of the section). The total length of the cross (L) was measured after counting the number of alveolar septum (Ns) laid on the cross. MLI (μm) = L/Ns.[2]

2.9. BALF cell counting and ELISA

The BALF was centrifuged at 1500 rpm at 4 °C for 10 min, and the cell pellet was resuspended in 500 μL PBS for differential counts of inflammatory cells with an automatic cell counter (Hitachi −7100, Japan).[21] The levels of inflammatory mediators such as TNF-α, IL-6, IL-1β, TGF-β, and mucin MUC5AC in serum and BALF were examined via ELISA according to the ELISA kit instructions (YX-E21175, YX-E21185, YX-E28867, YX-E21174, YX-E28780, Multisciences Biotech, Shanghai, China).

2.10. Western blot analysis

Lung tissue was lysed in ice-cold RIPA buffer for 40 min, followed by centrifugation at 12000×*g* for 30 min at 4 °C, and the supernatants were collected. The total protein concentration was then measured using a BCA protein analysis kit (Solarbio, Beijing, China). Protein denaturalization was performed at 100 °C for 10 min, and protein in the supernatant was separated by 10% twelve alkyl sulfate polyacrylamide gel electrophoresis (SDS–PAGE) (80 μg) and transferred to a polyvinylidene fluoride (PVDF) membrane (Millipore, Bedford, USA). The membrane was blocked with 5% milk buffer at room temperature, and the following primary antibodies were used at 4 °C overnight at a dilution of 1:1000: anti-rabbit p38 (CST, 9212S), anti-rabbit p-p38 (CST, 4511S), anti-rabbit ERK (CST, 4695S), anti-mouse *p*-ERK (CST, 9106S), anti-rabbit JNK (CST, 9252S), anti-rabbit *p*-JNK (CST, 4668S), anti-rabbit NF-κB (CST, 8242S), anti-rabbit p–NF–κB (CST, 3033S), anti-rabbit IκBα (abs131168), anti-rabbit *p*-IκBα (CST, 2859S), anti-rabbit TLR-2 (abs134064), anti-rabbit TLR-4 (abs132000), and anti-rabbit β-actin (BN0627). In TBST, the membrane was washed three times (10 min each) and then incubated with secondary antibody of goat anti-rabbit or anti-mouse immunoglobulin G (IgG) (dilution 1:2000) (Boster Biological Engineering, Wuhan, China) at room temperature for 1 h. The membrane was washed three times with TBST for 10 min/wash. Finally, signals were visualized using Super ECL Plus reagent (Solarbio, Beijing, China) and quantified by ChemiDocMP Imaging System (Bio-Rad Laboratories, Hercules, CA, USA) and ImageJ software.[22]

2.11. Quantitative real-time polymerase chain reaction (qRT–PCR)

The expression levels of MUC5AC, MUC5B, PI3K, AKT, and EGFR mRNA in the lung tissues were analyzed using quantitative real-time PCR (qPCR). The primers were designed and synthesized by Sangon Biotech (Shanghai, China).[23] The primer sequences used in this study are listed in Table 2. Total RNA was extracted using a total RNA extraction kit (Tiangen, China) according to the manufacturer's instructions. The First-Strand cDNA Synthesis Kit (Tiangen, China) was used for the reverse transcription process. The reaction systems were performed using an Applied Biosystems 7300 Fast Real-Time PCR System. The process of initial enzyme activation was set at 95 °C for 5 min, followed by 40 cycles of 95 °C for 10 s and 60 °C for 30 s. For qRT–PCR, Ct (threshold cycles) values were used to calculate the mRNA levels by formula $2^{-\Delta\Delta Ct} = 2^{-[\Delta Ct\ treatment\ -\Delta Ct\ control]}$.[24] The GAPDH level was used as a reference to normalize the expression levels of the other genes.

2.12. Flow cytometry

One hundred microliters of anticoagulant blood was added to 2 μL of FITC anti-rat CD4 (201505, Biolegend, USA), PE/Cyanine7 anti-rat CD8a (201716, Biolegend, USA), and APC anti-rat CD25 (202114, Biolegend, USA) and incubated for 30 min in the dark. Following incubation, 2 mL of red blood cell lysate (4203, Biolegend, USA) was added, and the reaction was conducted at room temperature for 10 min in the dark after gentle blowing and mixing. Then, the reaction mixture was centrifuged at 350 g for 5 min, the supernatant was discarded, and the precipitate was washed with 2 mL PBS with centrifugation at 350*g* for 5 min. The precipitate sample was detected by flow cytometry after disposal in 500 μL PBS. Data were collected using DxFLEX software (Beckman Coulter) with automatic compensation and were analyzed using FlowJo software (TreeStar, Ashland, OR).[25]

2.13. Statistical analysis

Statistical analyses were performed using GraphPad Prism 8.0 (GraphPad Software, USA). When necessary, the Prism8.0 statistical analysis program was used to do one-way analysis of variance (ANOVA)

Table 2
Primers sequences used for RT-qPCR.

Genes	Forward (5′–3′)	Reverse (5′–3′)
GAPDH	ACAGCAACAGGGTGGTGGAC	TTTGAGGGTGCAGCGAACTT
MUC5AC	CAACACACCACTGCAAGAGC	GGCTGTGTGGTAGCTGAAGT
MUC5B	CCTACGTGCCGCTCTCTAAG	CAGGCAGGTCAACTTCCCAT
EGFR	ACTGCGAGAACCAAGCTACT	GGAGGCTCAGAAAGTGGTCT
PI3K	GAACAGGGCAGCTTCAATGC	CTCCTTCTGGGTCCGGAGTA
Akt	CCTGGACTACTTGCACTCCG	CACAGCCCGAAGTCCGTTAT

followed by a Tukey's post hoc test for comparison among multiple groups or a Student's *t*-test for comparison between two groups (GraphPad). All values were expressed as the mean ± standard deviation (SD). $P < 0.05$ was considered to indicate a statistically significant difference.

3. Results

3.1. Identification of chemical constituents in AGKP

The chemical constituents of AGKP were tentatively characterized using UHPLC-Q-Orbitrap-HRMS based on accurate mass, MS/MS data, and characteristic fragmentation, referring to reference standards or related literature. A total of 90 chromatographic peaks were analyzed, and the corresponding compounds were characterized (Fig. 2A and B), including triterpenoids and saponins, flavonoids, anthracenes and derivatives, organic acids, phenylpropionic acids, and other compounds (Additional file 1: Table S1).

Taking peak 24 as an example to explain the major fragmentation pathways of flavonoids in AGKP, an accurate precursor ion of *m/z* 417.1191 $[M-H]^-$ ($C_{21}H_{22}O_9$, error 2.86 ppm) was observed in negative ion mode, as shown in Fig. 2C. The fragment of *m/z* 255.0662 [M-H-glucose]$^-$ was produced from the drop of a glucose aglycone. The characteristic fragments of liquiritigenin, such as *m/z* 135.0077, 119.0491 and 91.0176, were observed. Combined with the fragmentation pattern of the reference standard, peak 24 was identified as liquiritin. The cleavage of triterpenoid saponins and structural identification was illustrated by peak 46. A precursor ion of *m/z* 821.3059 $[M-H]^-$ ($C_{42}H_{62}O_{16}$, error 0.64 ppm) was obtained in negative ion mode. As shown in Fig. 2D, the fragments of *m/z* 425.3441 formed by the loss of two glucuronic acids as well as CO_2. The special fragment ions at *m/z* 351.0568, 193.0346 and 175.0238 were assignable to diglucuronic acid and monoglucuronic acid. Thus, peak 46 was identified as glycyrrhizic acid by comparison with the reference standard.

3.2. Network pharmacology predicts potential signaling pathways of AGKP in the treatment of COPD

A total of 886 targets of the 48 AGKP components (Additional file 2 Table S2) were predicted, and the component-target network was illustrated by Cytoscape 3.8.2 software. As shown in Fig. 3A, the network has 5058 lines and 934 nodes (comprising 48 components and 886 targets). The lines between the components (green quadrangles) and the targets (red circles) represented the interaction.

A total of 3125 common COPD targets were obtained by screening the following databases, including 462 targets in CTD, 42 in TCMIP, 2699 in Gene Cards and 700 in DiSGeNET. Among them, 596 were shared with 886 targets of AGKP components. Then, STRING was used to screen 596 shared targets with the criteria of "*Homo sapiens*" and "minimum required interaction score ≥0.999″, and 136 co-targets were obtained. There were some close associations among them, as shown in Fig. 3B. According to the network visualization analysis in Fig. 3C, androgen receptor (AR), estrogen receptor (ESR1), peroxisome proliferator-activated receptor gamma (PPARG), and transcription factor p65 (RELA) were the core therapeutic COPD targets of AGKP.

The DAVID database was used to perform GO and KEGG enrichment analyses on the common therapeutic COPD targets of AGKP. The enrichment of GO and KEGG terms and pathways is inversely correlated with the P value. A total of 1033 GO terms were obtained via GO enrichment analysis, including 137 in cellular component (CC), 172 molecular function (MF) terms, and 724 biological process (BP) terms. A total of 163 signaling pathways were acquired via KEGG enrichment analysis (Additional file 3 Tables S3 and 4). The top 10 GO terms and top 25 signaling pathways are displayed in Fig. 3D and E, respectively. The results indicated that the PI3K-Akt signaling pathway and MAPK signaling pathway were substantially enriched.

We performed molecular docking using the key therapeutic COPD targets as receptors and the 48 active components of AGKP as ligands. Receptors included AR (PDBID = 5U8Q), ESR1 (PDBID = 4XI3), PPARG (PDBID = 7AWC), and RELA (PDBID = 1VJ7). We evaluated the matching degree between the components and the key targets of AGKP

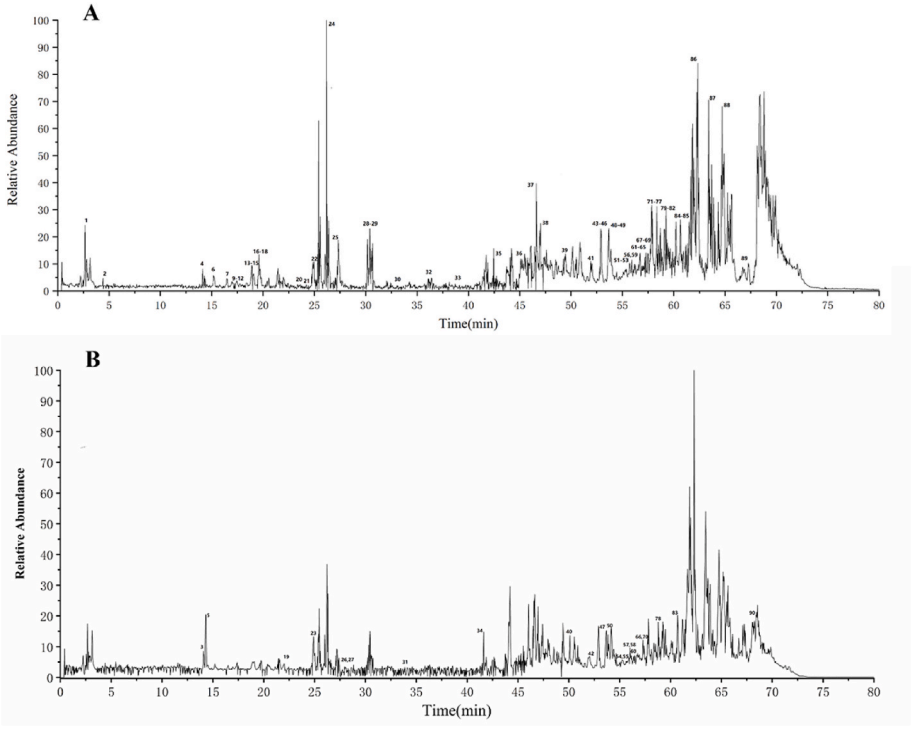

Fig. 2. The total ion current (TIC) chromatogram and fragmentation behaviour of representative compounds of AGKP. **A**: negative ion mode; **B**: positive ion mode; **C**: fragmentation behaviour of peak 24 (liquiritin); **D**: peak 46 (glycyrrhizic acid).

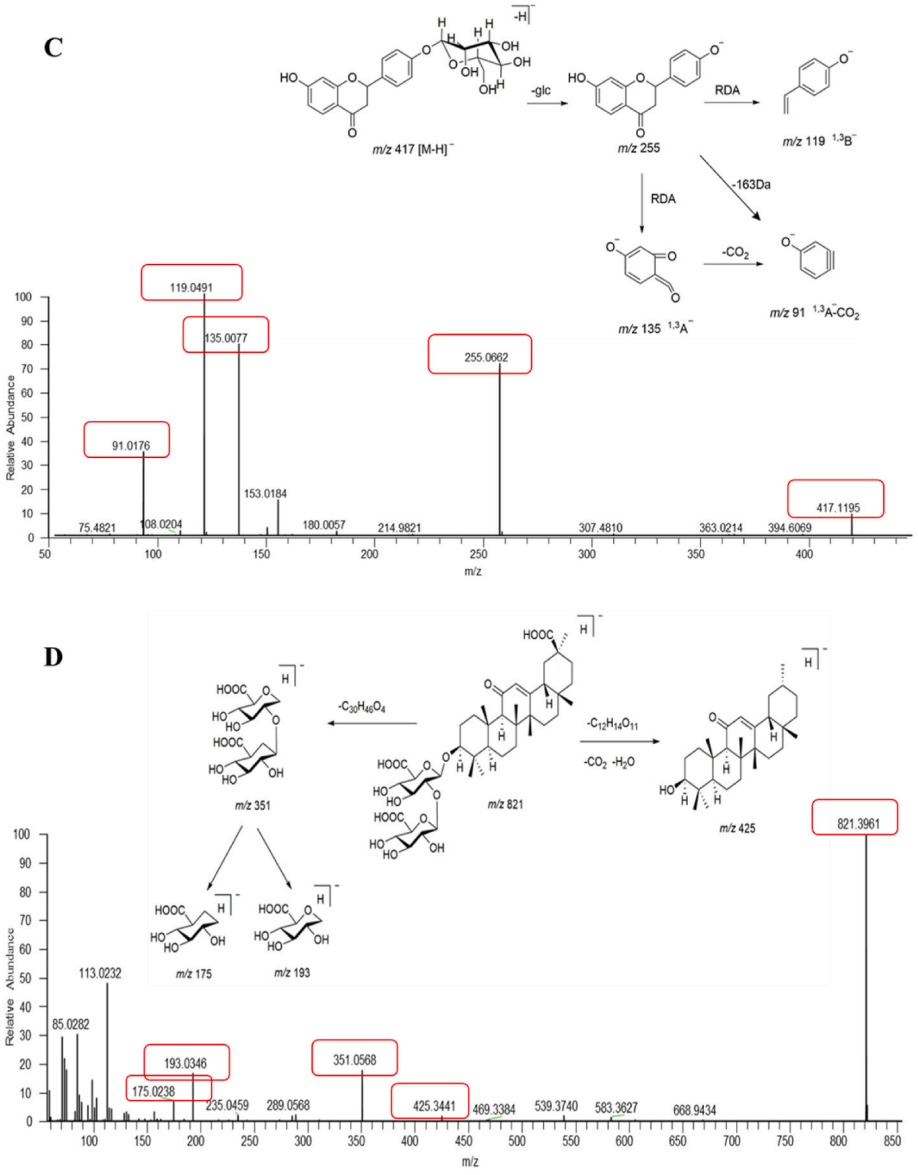

Fig. 2. (*continued*).

based on the magnitude of the binding energy. When the receptors and ligands are in stable conformations, it's more possible to bind if the energy is low. Then we evaluated the matching degree between the components and the key targets of AGKP based on the magnitude of the binding energy. When the receptors and ligands are in stable conformations, it's more possible to bind if the energy is low. Usually, binding energy ≤ -4.25 kcal/mol indicates certain binding between receptors and ligands, ≤-5.00 kcal/mol indicates good binding, and≤-7.00 kcal/mol indicates strong binding. According to the results shown in Fig. 3F and G, RELA (NF-κB p65) had suitable binding to AGKP components (Additional file 4 Table S5).

3.3. Effects of AGKP on pathological changes and pulmonary function

Measurement of the body weights was conducted once a week until the rats were sacrificed. As presented in Fig. 4A, there was a significant weight loss in rats treated with CS and LPS compared to control rats, while those treated AGKP, Mont or GK showed substantial improvements in body weight compared to the body weights of rats in the model group at 30 days. As shown in Fig. 4B, none of the rats in the control group died; in contrast, thirteen rats in the COPD model group succumbed during model creation (1, 5, 4, 2 and 1 rats succumbed at weeks 1, 2, 3, 4 and 5, respectively). However, AGKP treatment significantly improved the survival rate of COPD model rats induced by CS and LPS.

Pulmonary function test results showed that a downward trend was observed for TV, PEF, PIF and EF50, while an upward trend was observed for Penh and PAU in COPD model rats, in contrast with those of control group rats ($p < 0.05$, $p < 0.001$). The above indexes were significantly reversed in rats treated with different doses of AGKP, Mont, and GK compared with those in COPD model group rats (all, $p < 0.001$). Notably, there was a greater improvement in PEF function in the AGKP medium group than in both positive control groups (Fig. 4C).

The results of H&E staining of the lung tissue revealed that CS and LPS intervention induced obvious morphological changes and serious injuries in COPD model rats, including a significant increase in the infiltration of pulmonary tracheal epithelial cells, interstitial inflammatory cells around the lumen, expansion and fusion of alveoli, swelling of pulmonary bubbles and lung injury pathological scores. Administration of different doses of AGKP, Mont, and GK significantly reversed the above pathological changes ($p < 0.05$) (Fig. 4D). The MLI was obviously increased in COPD model group compared with control group ($p <$

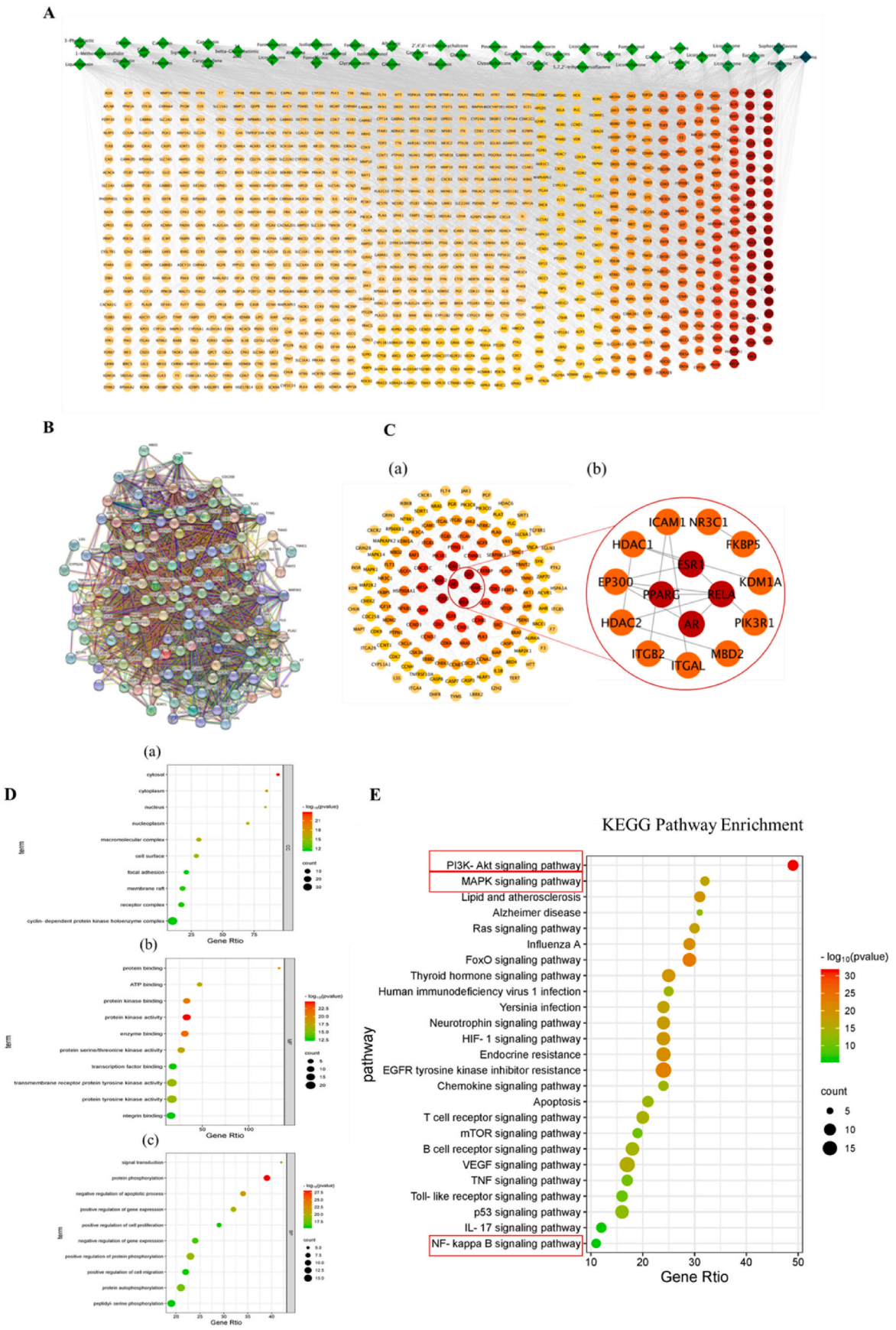

Fig. 3. The potential molecular mechanism of AGKP to treat COPD based on network pharmacology analysis and Molecular docking between the active ingredients and core proteins. **A**: AGKP network of compound-target with the targets (red circles) and the active compounds in the AGKP (green quadrangles); **B**: PPI network diagram; **C**: (a) the key targets of AGKP in the treatment of COPD; (b) The 4 targets in red represent the core targets. **D**: GO enrichment analysis of target proteins in

the PPI network, (a): Cellular component; (b): Molecular function; (c): Biological process; **E**: The top 25 enriched pathways in KEGG pathway analysis of the target proteins in the PPI network. **F**: Binding affinity between the major active ingredients and core targets (the darker the color, the stronger the binding activity of the receptor to the ligand); **G**: Docking results of 5-7-2′ trihydroxyisoflavone with AR (a); Docking results of 18-betta Glycyrrhetintic acid with ESR1 (b); Docking results of Xambioom with PPARG (c); Docking results of Sophoraisoflavone A with RELA (d).

0.001). However, the MLI was significantly decreased in the treatment groups compared with model group ($p < 0.001$, Fig. 4E).

3.4. AGKP suppresses LPS- and CS-induced pulmonary inflammation

Pulmonary inflammatory responses were evaluated by measuring the levels of inflammatory cells and proinflammatory cytokines. COPD model rats showed an obvious increase in the numbers of leukocytes, neutrophils, macrophages, and lymphocytes in BALF ($p < 0.001$). However, AGKP inhibited the infiltration of inflammatory cells in COPD model rats by decreasing the accumulation of these inflammatory cells in BALF (all, $p < 0.001$, Fig. 5A). As shown in Fig. 5B and C, there was a significant uptrend in pro-inflammatory cytokine levels of IL-1β, IL-6, TNF-α and TGF-β in the BALF and serum in COPD model rats compared with control group rats ($p < 0.001$). AGKP treatment significantly reduced the levels of the proinflammatory cytokines IL-1β, IL-6, TNF-α and TGF-β in the serum and BALF (all, $p < 0.001$). These results showed that AGKP protected against lung injury in COPD model rats from inflammation.

3.5. AGKP inhibited the activation of the PI3K/AKT and MAPK signaling pathways in COPD model rats

To further explore the underlying mechanisms of AGKP treatment on the inflammatory response in COPD model rats, the main signaling pathways PI3K/AKT and MAPK predicted by KEGG analysis, which have been shown to play an important role in inflammatory responses in COPD, were verified by PCR and western blotting. As shown in Fig. 6A–C, the mRNA levels of PI3K, AKT and EGFR in the AGKP treatment group were significantly higher than those in the COPD model group ($p < 0.001$). Similar results obtained from western blotting analysis indicated that the expression of phosphorylated levels of PI3K and AKT was upregulated in the lung tissues of COPD model rats but significantly down-regulated in those of AGKP-treated rats (Fig. 6D–F). Moreover, AGKP treatment significantly reduced the levels of phosphorylated p38, JNK, and ERK in lung tissues ($p < 0.001$) (Fig. 6G–J). These results indicated that AGKP could effectively protect lung tissues by inhibiting the activation of the PI3K/AKT and MAPK signaling pathways.

3.6. AGKP inhibited the activation of the TLR/NF-κB signaling pathway in COPD model rats

Based on the results of molecular docking analysis, NF-κB showed suitable binding affinity with AGKP components. Therefore, related proteins of TLR-4, TLR-2, IκB-α, and NF-κB were further examined by Western blot analysis. The AGKP treatment group showed an obvious reduction in the expression levels of TLR-4 and TLR-2 and the phosphorylation of NF-κB and IκB-α compared with those in the COPD model group ($p < 0.001$) (Fig. 6K-O).

3.7. AGKP inhibited MUC5AC and MUC5B gene expression and MUC5AC production in COPD model rats

To further explore the degrees of mucus hypersecretion, the mRNA levels of MUC5AC and MUC5B in lung tissue and the levels of MUC5AC in serum and BALF were measured by qRT-PCR and ELISA. As shown in Fig. 7A, MUC5AC production in serum and BALF in the COPD model group was significantly higher than that in the AGKP treatment group (all, $p < 0.001$). Moreover, the gene expression of MUC5AC and MUC5B was significantly down-regulated by AGKP treatment in COPD model rats ($p < 0.001$) (Fig. 7B). The inhibition level of AGKP on gene expression was greater than that of the positive control group ($p < 0.001$). These results suggested that AGKP could improve COPD by inhibiting the overproduction of mucus in airway cells.

3.8. Effect of AGKP on T-cell subsets in the blood of COPD model rats

As illustrated in Fig. 7C, the flow cytometry results indicated that AGKP treatment significantly increased the $CD4^+$, $CD8^+$, and $CD4^+/CD8^+$ T-cell subsets compared with the COPD model group. Although the percentage of $CD4^+CD25^+$ Treg cells among $CD4^+$ cells was significantly increased in the COPD model group, the results of the AGKP treatment group were not significantly different, and there was only a small reduction in the percentage of $CD4^+CD25^+$ Treg cells among $CD4^+$ cells. It was suggested that AGKP can increase the proportion of T-cell subsets in peripheral blood and enhance the immune response through $CD4^+$, $CD8^+$, and $CD4^+/CD8^+$ T cells.

4. Discussion

The pathogenesis of COPD is diverse and complex, in which inflammation and mucus hypersecretion are the main pathogenic factors in the development and progression of COPD.[26] COPD causes airway inflammation and bronchial tube narrowing, leading to mucus blocking and preventing air movement across the lungs.[27,28] Bronchodilators, corticosteroids, phosphodiesterase-4 inhibitors, and β2-agonists have commonly been used in clinical treatment to prevent COPD symptoms. Although these therapeutic methods have been applied to suppress to progression of COPD, most COPD patients are insensitive to these drugs. At present, glucocorticoids are one of the most popular anti-inflammatory medications, but most COPD patients have shown poor reactions to both oral and inhaled glucocorticoids, even at high doses.[29,30] AGKP relieves cough, resolves phlegm, and ameliorates asthma and is suitable for the treatment of various respiratory diseases. To our knowledge Guilong Kechuanning capsule is well-known traditional Chinese medicine formula which is widely used in the treatment of asthma and relieving the cough.[31] AGKP, like other traditional Chinese medicine, contains a large number of chemical components. In order to make the experimental data more representative and comparable, we have additionally applied Guilong Kechuanning capsule (State medical permit No. Z120053135) as a positive control.

Pulmonary function testing is used in clinical practice as a gold standard for the diagnosis and evaluation of COPD, as well as an important tool to detect the presence of air flow limitation. In this study, the successful establishment of a COPD model and the effect of AGKP on lung function were determined by assessing pulmonary function and morphological changes in lung tissue. Pulmonary function parameters such as TV, PEF, PIF, EF50, penh, and PAU reflect the severity of airway resistance and obstructive ventilation impairment.[17] Interestingly, the therapeutic effect of PEF in the medium and high-dose groups of AGKP was greater than that of the positive control group, which suggested that AGKP could more effectively improve ventilation function. A range of pathological alterations in lung tissues, which are characterized by parenchymal destruction and loss of alveolar attachments, contribute to airflow limitation.[32] Our experimental results showed that the lower the pulmonary function was, the more severe the lung injury. However, AGKP can reduce the pathological changes of lung injury in COPD model rats by alleviating the pathological state of pulmonary tracheal epithelial cells, interstitial inflammatory cells around the lumen, alveolar dilation and fusion, and alveolar swelling.

Continuous systemic and pulmonary inflammation has been thought

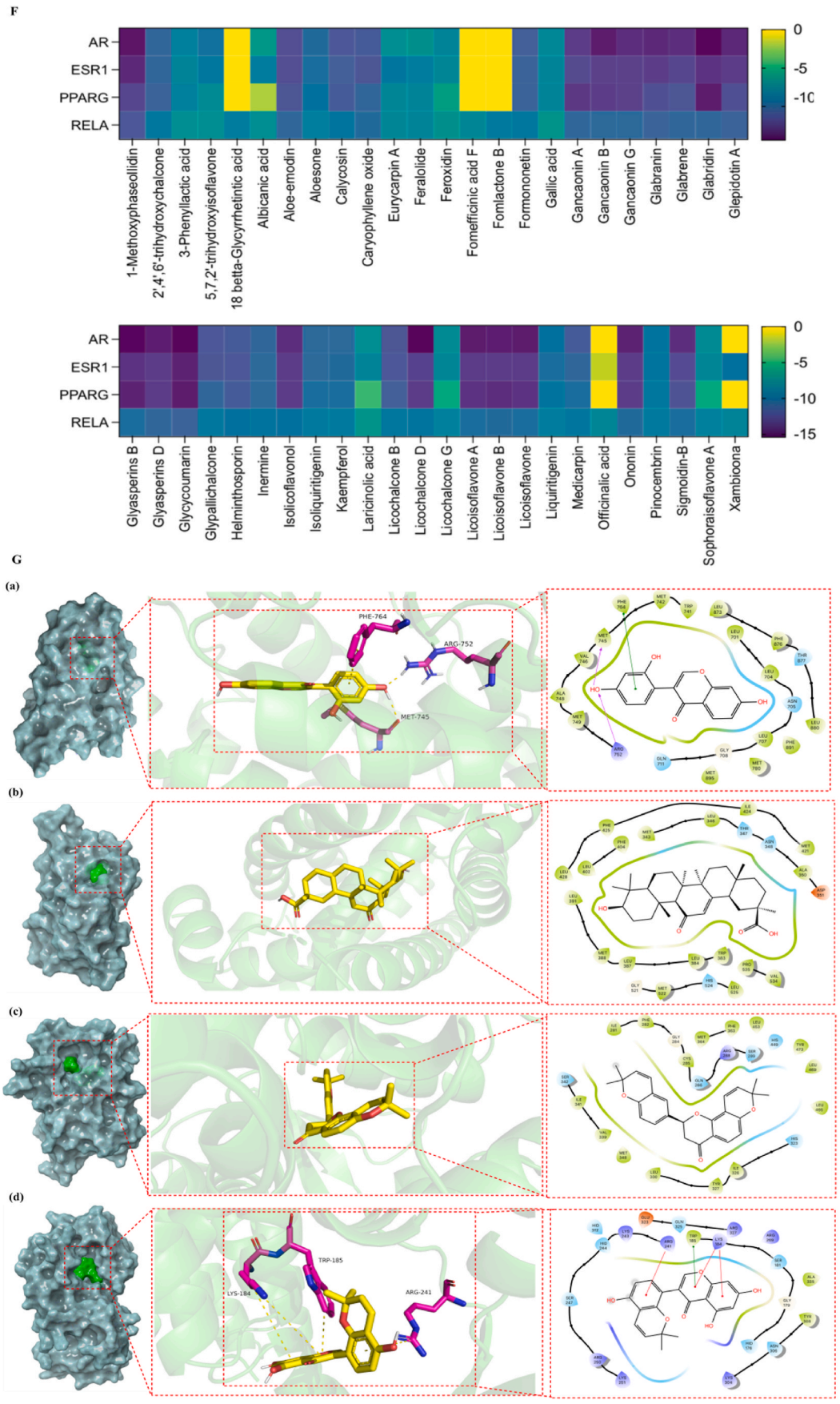

Fig. 3. (*continued*).

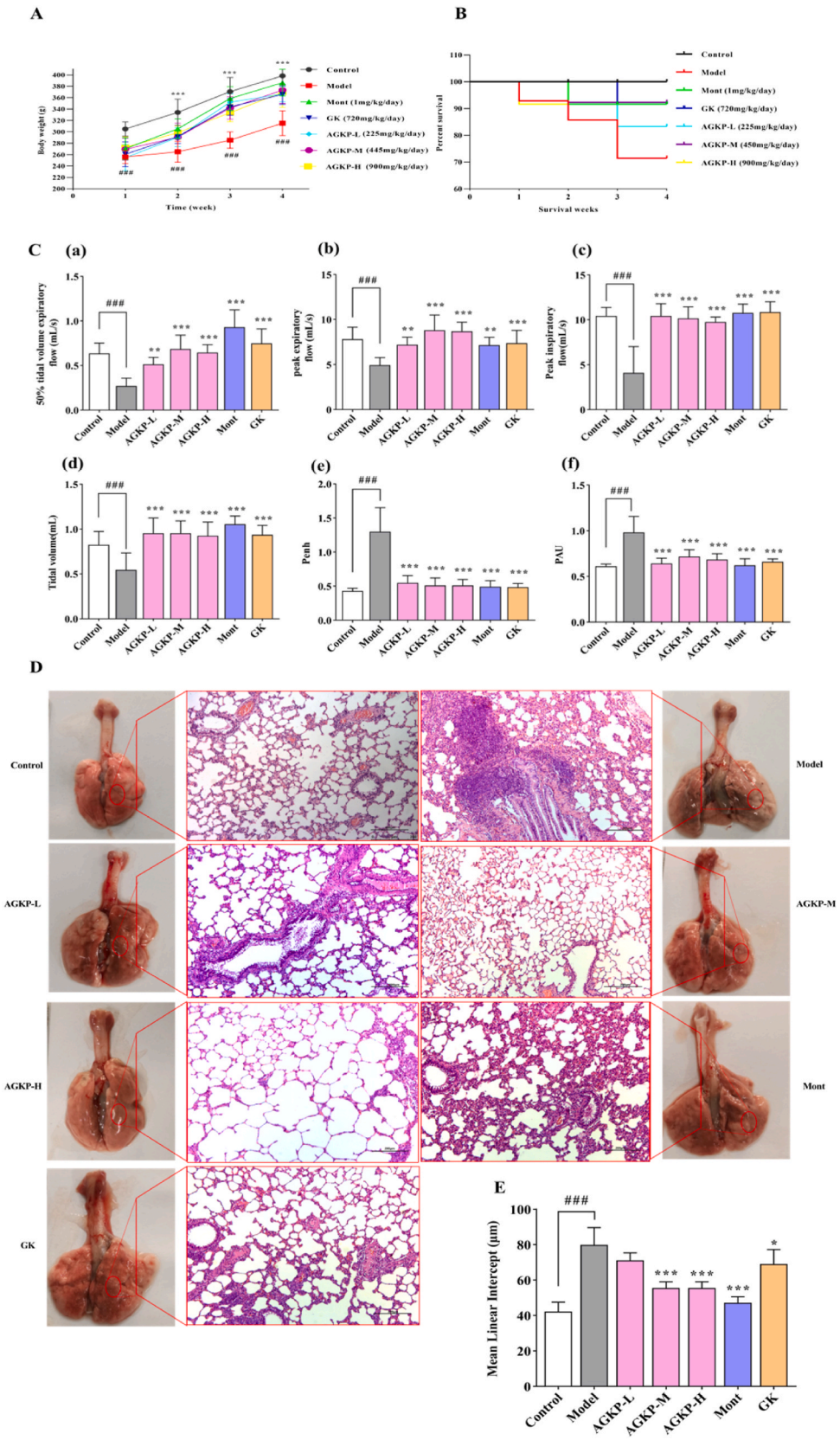

Fig. 4. The therapeutic effect of AGKP on LPS- and CS- induced COPD model rats. **A**: Body weight changes of during treatment; **B**: the survival rate; **C**: pulmonary function, (a) EF50; (b) PEF; (c) PIF; (d) TV; (e) Penh; (f) PAU; **D**: pathological changes (HE, x100); **E**: lung tissue injury. Data are expressed as mean ± SD, ($^{\#}$ compared to control, $^{\#\#\#}p < 0.001$; * compared to model * $p < 0.05$, **$p < 0.01$, ***$p < 0.001$) ($n = 12$).

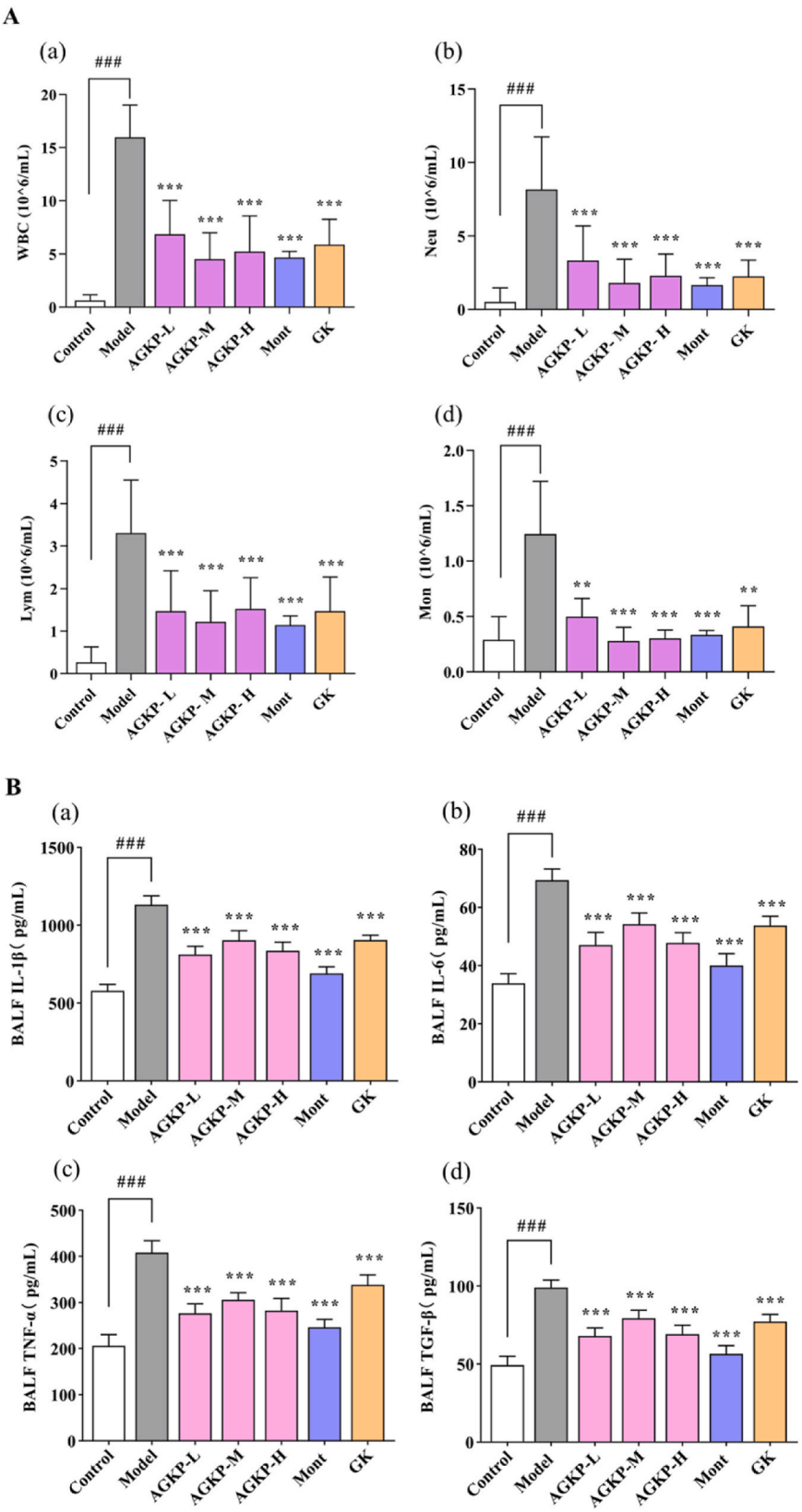

Fig. 5. AGKP suppresses LPS- and CS-induced pulmonary inflammation. **A**: Inflammatory cells (a: WBC, white blood cells; b: NEU, neutrophils; c: LYM; d: MON, monocyte.) in BALF. **B:** Pro-inflammatory cytokines in the BALF (a: Levels of IL-1β; b: Levels of IL-6; c: Levels of TNF-α; d: Levels of TGF-β). **C:** Pro-inflammatory cytokines in the serum (a: Levels of IL-1β; b: Levels of IL-6; c: Levels of TNF-α; d: Levels of TGF-β). The results are expressed as mean ± SD ($^{\#}$ compared to control, $^{\#\#\#}p < 0.001$; * compared to model * $p < 0.05$, **$p < 0.01$, ***$p < 0.001$) ($n = 8$).

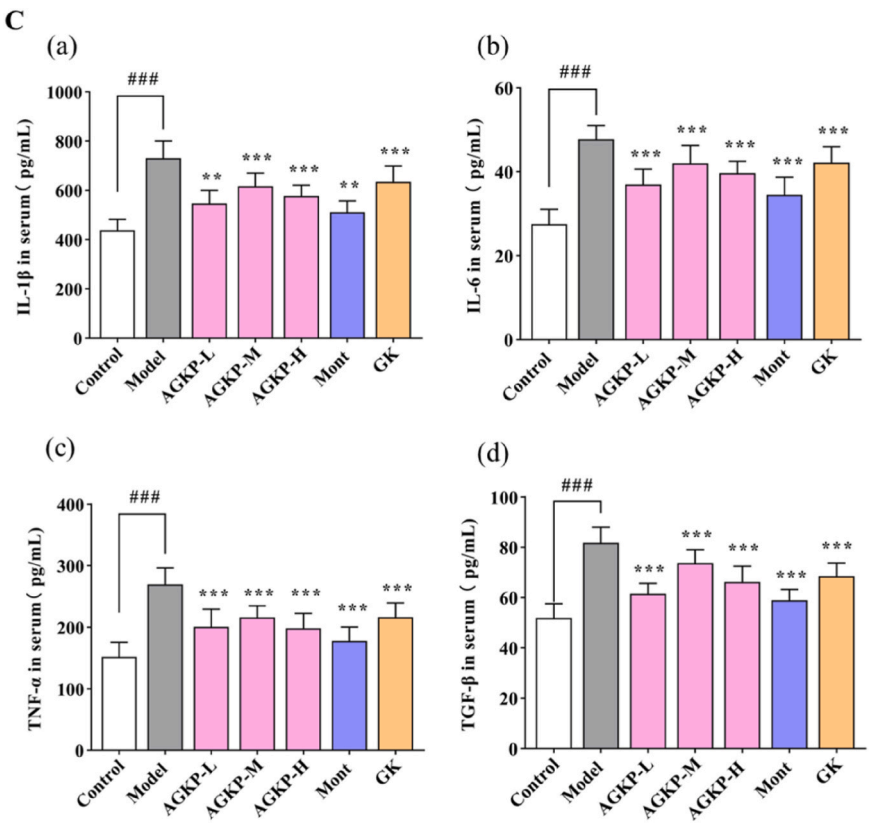

Fig. 5. (*continued*).

to be another cause factor of COPD onset and development. With the progression of COPD, more macrophages, neutrophils and inflammatory mediators infiltrate the airways and lung parenchyma, resulting in the inflammatory response by strengthening cell signaling.[33] The count of inflammatory cells with or without AGKP was measured to further investigate the anti-inflammatory effects of AGKP in COPD model rats. Moreover, cytokines are involved in immune and inflammatory responses. IL-1β and TNF-α play vital roles during the occurrence and enhancement of the inflammatory response.[16,34] Studies have shown that inflammatory cells, particularly neutrophils, play a significant role in the secretion of cytokines.[35] In clinical trials, neutrophils were the main cells infiltrating the lung and secreting TNF-α, IL-6, and IL-1β.[36] Therefore, the ability to inhibit cytokine release is an important indicator of anti-inflammatory activity. In our research, we also found that AGKP therapy markedly decreased inflammatory cell accumulation in the BALF of COPD model rats through marked inhibition of TNF-α, IL-1β, TGF-β and IL-6. Based on the UHPLC–MS analysis results and molecular docking results, flavonoids from AGKP, such as isoliquiritigenin, glycyrrhizic acid, 18 β-glycyrrhetinic acid, were bioactive components, which suggests that these components likely contribute to the therapeutic effect of AGKP on COPD. Relevant reports also support our experimental that these compounds have good anti-inflammatory effects.[14,37] We also found that some compounds with better molecular docking binding, such as isoliquiritigenin, were used to treat CS-induced COPD animal models as effective antioxidants and anti-inflammatory agents via the regulation of the Nrf2 and NF-κB Signaling Pathways.[38] We can speculate from these results that AGKP may have potential therapeutic effects against the development of LPS- and CS-induced COPD due to its reduction in the recruitment of inflammatory cells and the expression levels of inflammatory mediators.

The PI3K-AKT signaling pathway was the most enriched KEGG pathway. PI3K may be one of the key factors leading to the occurrence of airway inflammation. Previous reports have shown that LPS and CS induce an increase in PI3K and AKT phosphorylation in COPD model rats.[17,39] Our research indicated that AGKP treatment significantly inhibited the phosphorylation of PI3K and AKT, especially at high doses. AGKP most likely controls the PI3K-AKT pathway to restore the balance of the inflammatory response. Studies have shown that mucus hypersecretion in COPD is inhibited by inhibiting EGFR-PI3K-AKT signaling pathway.[40] The experimental results showed that AGKP inhibited mucus hypersecretion (MUC5AC). It was further verified that the inhibitory effect of AGKP on mucus hypersecretion was possibly related to the inhibitory effect of EGFR-PI3K-AKT.

MAPK activation is involved in the exacerbation of the inflammatory response, making the MAPK signaling pathway a potential target for anti-inflammatory therapy.[41] In COPD, inhibition of MAPK signaling effectively reduces airway inflammation.[16] This research supported previous findings that LPS and CS induction can contribute to the activation of the MAPK pathway, leading to phosphorylation of P38, ERK, and JNK and thereby upregulating the expression of proinflammatory cytokines. However, AGKP may reduce the release of inflammatory mediators by preventing activation of the MAPK signaling pathway, thereby alleviating inflammation in COPD.

Activation of the TLR4 signaling pathway can strongly trigger the release and production of various inflammatory factors and cytokines. NF-κB is also a key molecule of the Toll-like receptor 4 (TLR4) signal transduction pathway. Our study found that the expression levels of TLR4 and TLR2 were remarkably decreased in the AGKP treatment groups, and AGKP treatment had similar effects to Mont treatment at high and medium doses. In addition, NF-κB is a transcriptional regulator that induces the expression of many proinflammatory genes, as well as a key molecule of the TLR4 signal transduction pathway. Phosphorylation of IκB-α leads to cytoplasmic NF-κB translocation to the nucleus and results in transcription of proinflammatory genes, which play a crucial role in the inflammatory process of COPD.[42] The molecular docking results of this study showed that the active component of AGKP has

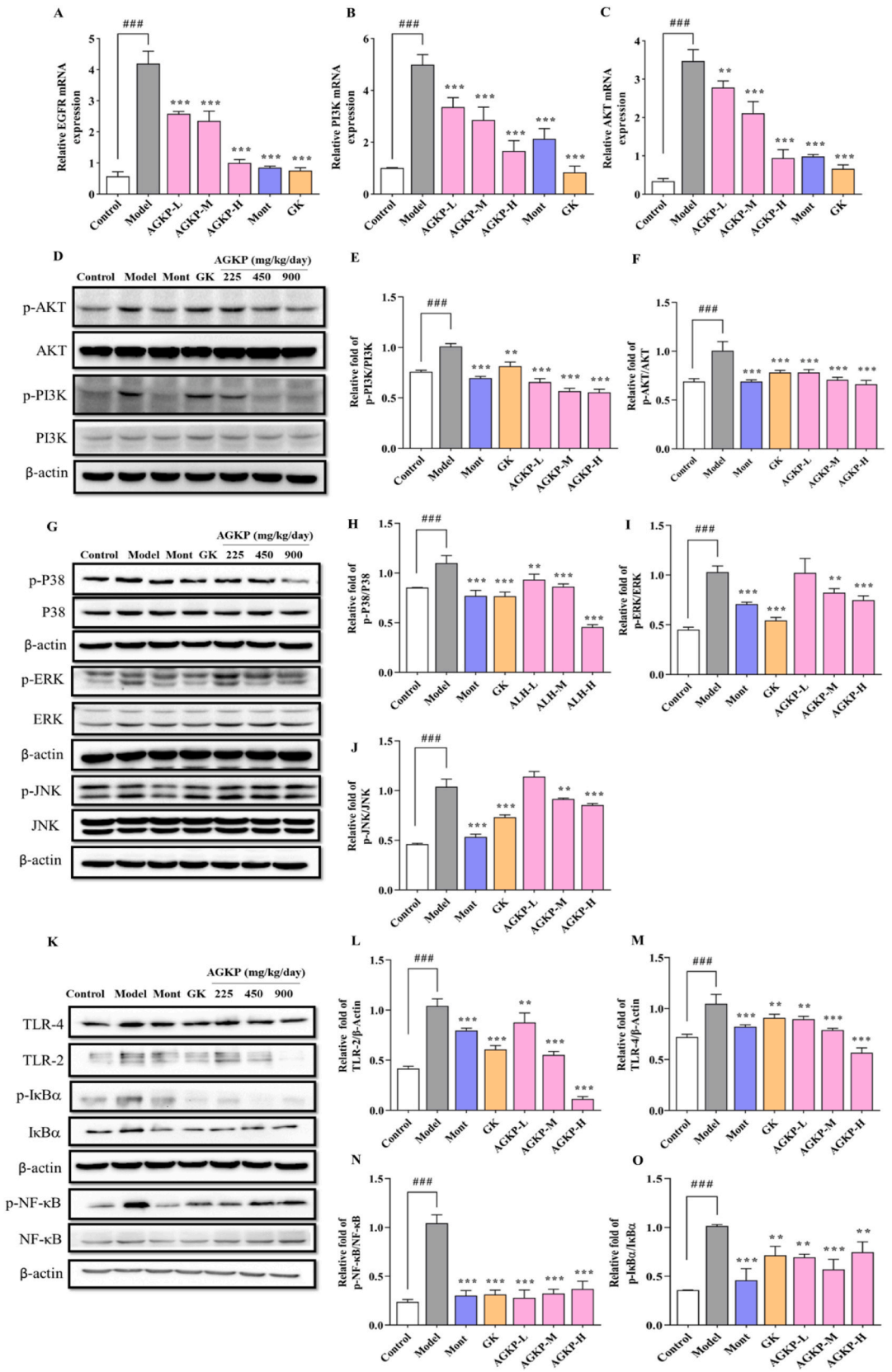

Fig. 6. AGKP exerts anti-inflammatory effects through inhibiting the expression of related proteins in the TLRs/PI3K/NF-κB, MAPK signaling pathways. **A-C**: The mRNA levels of EGFR, PI3K, AKT; **D-O**: The protein levels of p-PI3K, *p*-AKT, p-P38, *p*-ERK, *p*-JNK, TLR-2, TLR-4, p–NF–κB, *p*-IκBα; Data are expressed as mean ± SD, ($^{\#}$ compared to control, $^{\#\#\#}p < 0.001$; * compared to model * $p < 0.05$, ** $p < 0.01$, *** $p < 0.001$) ($n = 3$).

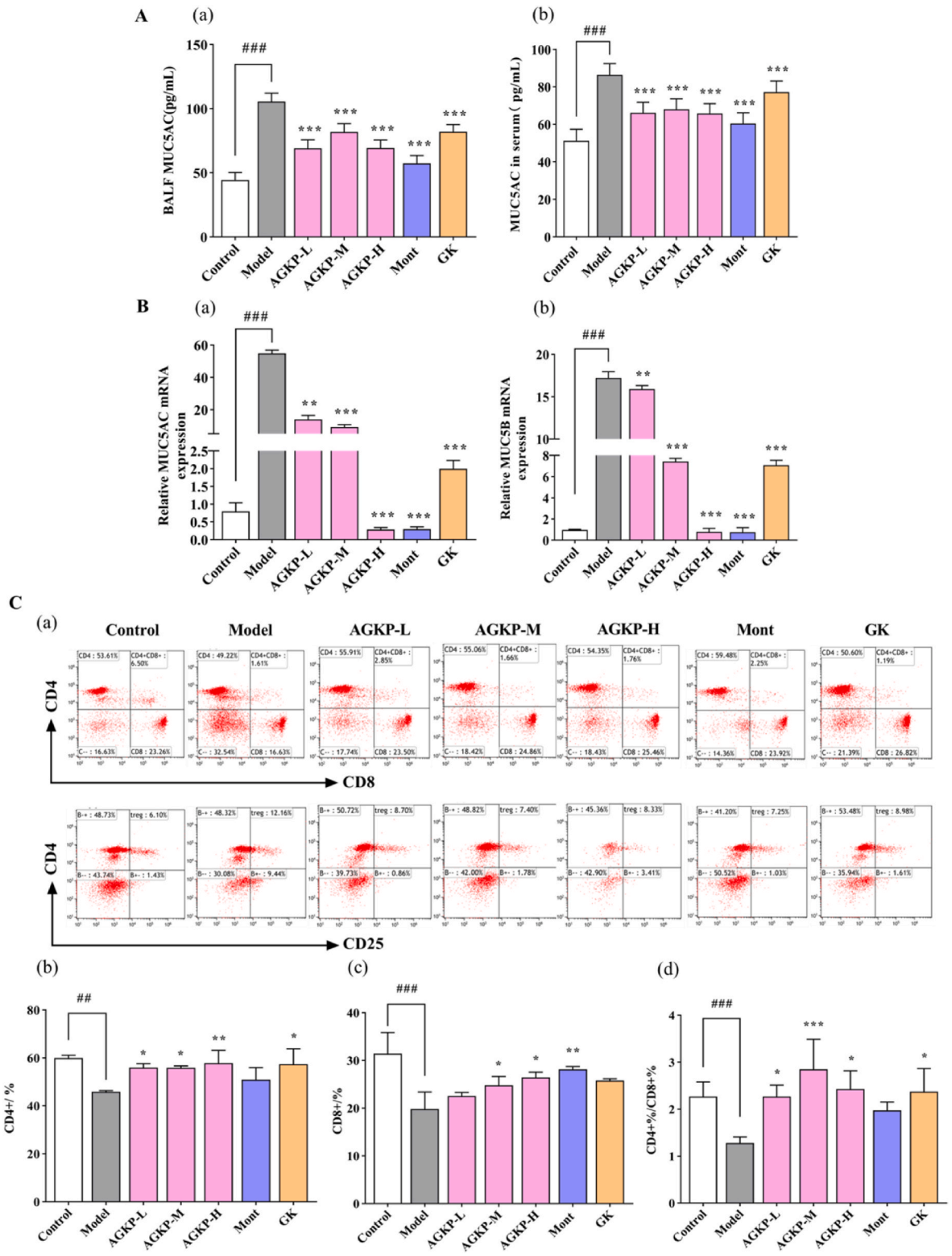

Fig. 7. Effect of AGKP on mucus hypersecretion and T cell subsets.
A: MUC5AC levels in the BALF (a) and serum (b) ($n = 8$); **B**: MUC5AC and MUC5B mRNA levels in the Lung tissue ($n = 3$); **C**: The proportion of T cell subsets (a); Statistics the proportion of $CD4^+$(b); Statistics the proportion of $CD8^+$(c); Statistics the proportion of $CD4^+/D8^+$(d). Data are expressed as mean ± SD, ($^{\#}$ compared to control, $^{\#\#\#}p < 0.001$; * compared to model * $p < 0.05$, **$p < 0.01$, ***$p < 0.001$).

suitable binding affinity to NF-κB p65 (RELA). Our results showed that LPS and CS exposure can contribute to the activation of the NF-κB pathways, leading to the phosphorylation of NF-κB and IκB. AGKP can inhibit the activation of the NF-κB pathways and reduce the expression levels of inflammation-related proteins, such as NF-κB and IκB-α. In summary, AGKP exerts its therapeutic effects by regulating the TLR/PI3K/NF-κB and MAPK signaling pathways (Fig. 8).

Mucus hypersecretion is closely related to airway limitation and

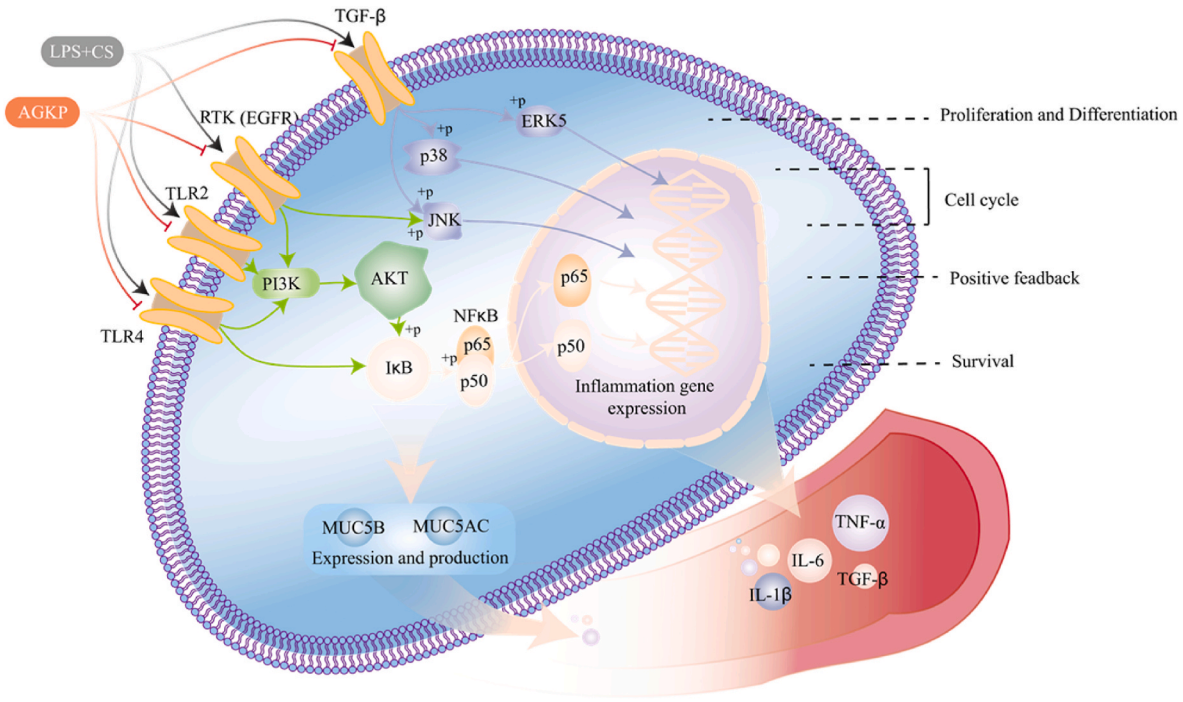

Fig. 8. A proposed schematic mechanism of AGKP in inhibiting LPS- and CS-induced inflammation in COPD rats.

pulmonary function decline in COPD patients. With the aggravation of airway inflammation, the expression of MUC5AC and MUC5B is upregulated.[43] Thus, the inhibition of mucus hypersecretion is a promising therapeutic strategy for asthma and COPD.[44] Our results showed that AGKP inhibited MUC5AC and MUC5B expression levels by suppressing NF-κB pretranscriptional activity, leading to decreased NF-κB binding to the MUC5AC promoter region in LPS- and CS-induced COPD model rats. AGKP was significantly more effective than GK at controlling MUC5AC production in COPD model rats, while the reduction in the levels of MUC5AC and MUC5B genes at high doses of AGKP was equivalent to that in Mont-treated rats. The above experimental results suggested that the inhibitory effect of AGKP on mucus hypersecretion may be related to its anti-inflammatory role in COPD model rats. Previous studies reported that triterpenoid compounds such as scutellarin in *Erigeron breviscapus* and salidroside in *Rhodiola* have expectorant activity by inhibiting the secretion of MUC5AC and are widely used clinically as expectorants.[45,46] LC–MS analysis indicated that AGKP is rich in triterpenoids. Therefore, we believe that triterpenoids from AGKP are likely to participate in the inhibition of mucus hypersecretion in COPD model rats.

Moreover, the regulation of Treg cell balance has been shown to play a key role in the anti-COPD effect according to previous studies.[47] Treg cells are present in the lung, and their effector functions include the attraction and enhancement of inflammatory function in other inflammatory cells, such as neutrophils and macrophages. Considerable neutrophil infiltration occurs in the inflamed lung of COPD patients.[48] Our results showed that the levels of immune cells in the blood of COPD model rats can affect the immune response. Exacerbations of COPD were positively correlated with lung T lymphocyte infiltrates but negatively correlated with the percentage of circulating $CD4^+$ and $CD8^+$ T lymphocytes.[49] In our research, AGKP significantly increased $CD4^+$, $CD8^+$ and $CD4^+/CD8^+$ levels in blood, suggesting that AGKP can increase peripheral blood T-cell subsets and enhance the immune response. In conclusion, AGKP, as a traditional Chinese medicine, displays multitarget and multipathway effects with its diverse chemical composition acting on different pathways associated with COPD, resulting in improved lung function, inflammation and mucus hypersecretion.

AGKP improves the progression of COPD through multi-component, multi-target and multi-pathway, which is different from chemical drugs acting on a single target. We can well understand the complex interaction between chemical components of traditional Chinese medicine and diseases by identifying network targets and signaling pathways. However, it is worth noting that this study has some limitations. First, since we have verified some of the core pathways and targets of AGKP, the results may be slightly skewed. Therefore, other related targets and signaling pathways predicted by network pharmacology need to be further verified in future experiments. Secondly, our study did not prove the association between mucus hypersecretion and inflammation. In subsequent experiments, we will test the relationship between them through in vitro experiments.

5. Conclusion

This study integrated UHPLC–MS compound component detection, network pharmacological analysis, and animal experiments to show that the pharmacological effect of AGKP against COPD may occur via the TLR/PI3K/NF-κB and MAPK signaling pathways to improve pulmonary function and lung histopathology, reduce inflammation, enhance the immune response and inhibit mucin hypersecretion. Our research provides a pharmacological and biological basis for the therapeutic effect of AGKP on patients suffering from COPD.

Funding

This work was financially supported by the National Key R&D Program of China (Grant No. 2020YFE0205600), Biological Resources Programme, Chinese Academy of Sciences (NO. KFJ-BRP-007-011), Xinjiang Science and Technology Major Project (NO. 2022A03018), and "CAM Resources DataBase" in National Basic Science Data Center (NO.NBSDC-DB-19).

Highlights of the findings and novelties

Agarikon pill (AGKP) improved lung function in COPD animal mode; AGKP down-regulated inflammatory factor levels in COPD rats; Network pharmacology analyses were performed; AGKP inhibited mucin hypersecretion; AGKP inhibited the PI3K/AKT, NF-κB and MAPK signaling

pathways relevant proteins.

Ethics approval and consent to participate

The animal study was reviewed and approved by Ethics Committee of Xinjiang Medical University (approval No. IACUC-20210315-17).

Declaration of competing interest

The authors declare that they have no known competing financial interests or personal relationships that could have appeared to influence the work reported in this paper.

Acknowledgments

Not applicable.

Appendix A. Supplementary data

Supplementary data to this article can be found online at https://doi.org/10.1016/j.jtcme.2024.03.006.

References

1. Global Initiative for Chronic Obstructive Lung Disease. *Global Strategy for the Diagnosis, Management, and Prevention of Chronic Obstructive Pulmonary Disease*. 2022.
2. Ma J, Tian Y, Li J, et al. Effect of bufei yishen granules combined with electroacupuncture in rats with chronic obstructive pulmonary disease via the regulation of TLR-4/NF-κB signaling. *Evid Based Complement Alternat Med*. 2019; 2019, 6708645.
3. Li S, Li J, Wang M, et al. Effects of comprehensive therapy based on traditional Chinese medicine patterns in stable chronic obstructive pulmonary disease: a fourcenter, open-label, randomized, controlled study. *BMC Compl Alternative Med*. 2012;12:197.
4. Fan Y, Wen X, Zhang Q, et al. Effect of traditional Chinese medicine bufei granule on stable chronic obstructive pulmonary disease: a systematic review and meta-analysis based on existing evidence. *Evid Based Complement Alternat Med*. 2020;2020, 3439457.
5. Jasemi SV, Khazaei H, Momtaz S, et al. Natural products in the treatment of pulmonary emphysema: therapeutic effects and mechanisms of action. *Phytomedicine*. 2022;99, 153988.
6. Zhou R, Luo F, Lei H, et al. Liujunzi Tang, a famous traditional Chinese medicine, ameliorates cigarette smoke-induced mouse model of COPD. *J Ethnopharmacol*. 2016;193:643–651.
7. Li Q, Wang G, Xiong S, et al. Bu-Shen-Fang-Chuan formula attenuates cigarette smoke-induced inflammation by modulating the PI3K/Akt-Nrf2 and NF-κB signalling pathways. *J Ethnopharmacol*. 2020;261, 113095.
8. Gaffey K, Reynolds S, Plumb J, et al. Increased phosphorylated p38 mitogen-activated protein kinase in COPD lungs. *Eur Respir J*. 2013;42(1):28–41.
9. Wang W, Wu W, Wang B, et al. Effect of houttuynia on improving lung injury in chronic obstructive pulmonary disease by regulating the TLR4 signaling pathway. *Food Sci Nutr*. 2021;9(7):3389–3396.
10. Jing LD, Su SS, Zhang DJ, et al. Srolo Bzhtang, a traditional Tibetan medicine formula, inhibits cigarette smoke induced airway inflammation and muc5ac hypersecretion via suppressing IL-13/STAT6 signaling pathway in rats. *J Ethnopharmacol*. 2019;235:424–434.
11. Song Y, Wang W, Xie YQ, et al. Carbocisteine inhibits the expression of Muc5b in COPD mouse model. *Drug Des Dev Ther*. 2019;13:3259–3268.
12. Li JS, Xie Y, Zhao P, et al. A Chinese herbal formula ameliorates COPD by inhibiting the inflammatory response via downregulation of p65, JNK, and p38. *Phytomedicine*. 2021;83, 153475.
13. Li YT, Zhao J, Shao H, et al. Preventive effect of total flavonoids of Trollius altaicus on a chronic obstructive pulmonary disease rat model based on the TLR4/NF-kappaB pathway. *Ann Transl Med*. 2022;10(4):222.
14. Kato K, Chang EH, Chen Y, et al. MUC1 contributes to goblet cell metaplasia and MUC5AC expression in response to cigarette smoke in vivo. *Am J Physiol Lung Cell Mol Physiol*. 2020;319(1):L82–L90.
15. *Standard for Prescriptions of Uygur Medical Institutions in Xinjiang Uygur Autonomous Region*. first ed. Urumqi: Xinjiang People's Publishing House; 2013.
16. China Pharmacopoeia Committee. *Drug Standard of Ministry of Public Health of the Peoples Republic of China-Uygur Medicine Volume*. Urumqi: Xinjiang science and Technology Health Publishing House; 1998.
17. Cai M, Xu Y, Deng B, et al. Radix Glycyrrhizae extract and licochalcone a exert an anti-inflammatory action by direct suppression of toll like receptor 4. *J Ethnopharmacol*. 2023;302(PtA), 115869.
18. Abudumijiti G, Shabiti S, Cong Y, et al. [Triterpenic acid of Fomesofficinalis Ames attenuates LPS-induced acute lung injury in mice via Nrf2 pathway]. *Zhong Guo Bing Li Sheng Li Za Zhi*. 2021;37(1):112–118.
19. Abulizi A, Simayi J, Nuermaimaiti M, et al. Quince extract resists atherosclerosis in rats by down-regulating the EGFR/PI3K/Akt/GSK-3beta pathway. *Biomed Pharmacother*. 2023;160, 114330.
20. Huang WJ, Wen F, Ruan S, et al. Integrating HPLC-Q-TOF-MS/MS, network pharmacology and experimental validation to decipher the chemical substances and mechanism of modified Gui-shao-liu-jun-zi decoction against gastric cancer. *J Tradit Complement Med*. 2023;13(3):245–262.
21. Li QP, Sun J, Cao YX, et al. Bu-Shen-Fang-Chuan formula attenuates T-lymphocytes recruitment in the lung of rats with COPD through suppressing CXCL9/CXCL10/CXCL11-CXCR3 axis. *Biomed Pharmacother*. 2020;123, 109735.
22. Duan XM, Li J, Cui JX, et al. Anti-inflammatory activity of Anchusa italica Retz. in LPS-stimulated RAW264.7cells mediated by the Nrf2/HO-1, MAPK and NF-κB signaling pathways. *J Ethnopharmacol*. 2022;286, 114899.
23. Li JS, Ma JD, Tian YG, et al. Effective-component compatibility of Bufei Yishen formula II inhibits mucus hypersecretion of chronic obstructive pulmonary disease rats by regulating EGFR/PI3K/mTOR signaling. *J Ethnopharmacol*. 2020;257, 112796.
24. Schmittgen TD, Livak KJ. Analyzing Real-time PCR data by the comparative CT method. *Nat Protoc*. 2008;3(6):1101–1108.
25. Zhao P, Liu XF, Dong HR, et al. Bufei yishen formula restores Th17/treg balance and attenuates chronic obstructive pulmonary disease via activation of the adenosine 2a receptor. *Front Pharmacol*. 2020;11:1212.
26. Yu N, Sun YT, Su XM, et al. Treatment with eucalyptol mitigates cigarette smoke-induced lung injury through suppressing ICAM-1 gene expression. *Biosci Rep*. 2018; 38(4), BSR20171636.
27. Li J, Qiu C, Xu P, et al. Casticin improves respiratory dysfunction and attenuates oxidative stress and inflammation via inhibition of NF-κB in a chronic obstructive pulmonary disease model of chronic cigarette smoke-exposed rats. *Drug Des Dev Ther*. 2020;14:5019–5027.
28. Tian YG, Li JS, Li Y, et al. Effects of bufei yishen granules combined with acupoint sticking therapy on pulmonary surfactant proteins in chronic obstructive pulmonary disease rats. *BioMed Res Int*. 2016;2016, 8786235.
29. Barnes PJ, Celli BR. Systemic manifestations and comorbidities of COPD. *Eur Respir J*. 2009;33(5):1165–1185.
30. Deng YX, Zhong J, Liu ZJ, et al. Active ingredients targeting Nrf2 in the Mongolian medicine Qiwei Putao powder: systematic pharmacological prediction and validation for chronic obstructive pulmonary disease treatment. *J Ethnopharmacol*. 2021;265, 113385.
31. Pan LY, Han YQ, Wang YZ, et al. Mechanism of Yanghe Pingchuan granules treatment for airway remodeling in asthma. *Drug Des Dev Ther*. 2018;12:1941–1951.
32. Fricker M, Deane A, Hansbro PM. Animal models of chronic obstructive pulmonary disease. *Expet Opin Drug Discov*. 2014;9(6):629–645.
33. Shin NR, Ryu HW, Ko JW, et al. A standardized bark extract of Pinus pinaster Aiton (Pycnogenol®) attenuated chronic obstructive pulmonary disease via Erk-sp1 signaling pathway. *J Ethnopharmacol*. 2016;194:412–420.
34. Li PF, Wang JK, Wang CG, et al. Therapeutic effects and mechanisms study of Hanchuan Zupa Granule in a Guinea pig model of cough variant asthma. *J Ethnopharmacol*. 2021;269, 113719.
35. Shin IS, Shin NR, Park JW, et al. Melatonin attenuates neutrophil inflammation and mucus secretion in cigarette smoke-induced chronic obstructive pulmonary diseases via the suppression of Erk-Sp1 signaling. *J Pineal Res*. 2015;58(1):50–60.
36. Jiang ZL, Zhu L. Update on molecular mechanisms of corticosteroid resistance in chronic obstructive pulmonary disease. *Pulm Pharmacol Ther*. 2016;37:1–8.
37. Kim YW, Zhao RJ, Park SJ, et al. Anti-inflammatory effects of liquiritigenin as a consequence of the inhibition of NF-kappaB-dependent iNOS and proinflammatory cytokines production. *Br J Pharmacol*. 2008;154(1):165–173.
38. Yu D, Liu XB, Zhang GX, et al. Isoliquiritigenin inhibits cigarette smoke-induced COPD by attenuating inflammation and oxidative stress via the regulation of the Nrf2 and NF-κB signaling pathways. *Front Pharmacol*. 2018;9:1001.
39. Xu F, Lin JP, Cui WQ, et al. Scutellaria baicalensis attenuates airway remodeling via PI3K/akt/NF-kappaB pathway in cigarette smoke mediated-COPD rats model. *Evid Based Complement Alternat Med*. 2018;2018, 1281420.
40. Feng F, Du J, Meng Y, Guo F, Feng C. Louqin zhisou decoction inhibits mucus hypersecretion for acute exacerbation of chronic obstructive pulmonary disease rats by suppressing EGFR-PI3K-AKT signaling pathway and restoring Th17/treg balance. *Evid Based Complement Alternat Med*. 2019;2019:1–14.
41. Li CL, Shi Q, Yan Y, et al. Recuperating lung decoction attenuates the oxidative stress state of chronic obstructive pulmonary disease by inhibiting the MAPK/AP-1 signal pathway and regulating γ-GCS. *Evid Based Complement Alternat Med*. 2017; 2017, 9264914.
42. Ghosh S, Karin M. Missing pieces in the NF-kB puzzle. *Cell*. 2002;109(Suppl): S81–S96.
43. Radicioni G, Ceppe A, Ford AA, et al. Airway mucin MUC5AC and MUC5B concentrations and the initiation and progression of chronic obstructive pulmonary disease: an analysis of the SPIROMICS cohort. *Lancet Respir Med*. 2021;9(11): 1241–1254.
44. Nakao I, Kanaji S, Ohta S, et al. Identification of pendrin as a common mediator for mucus production in bronchial asthma and chronic obstructive pulmonary disease. *J Immunol*. 2008;180(9):6262–6269.
45. Jiang DP, Perelman JM, Kolosov VP, et al. Effects of scutellarin on MUC5AC mucin production induced by human neutrophil elastase or Interleukin 13 on airway epithelial cells. *J Kor Med Sci*. 2011;26(6):778–784.
46. Li Q, Zhou XD, Kolosov VP, et al. Salidroside reduces cold-induced mucin production by inhibiting TRPM8 activation. *Int J Mol Med*. 2013;32(3):637–646.
47. Sileikiene V, Laurinaviciene A, Lesciute-Krilaviciene D, et al. Levels of CD4+ CD25+ T regulatory cells in bronchial mucosa and peripheral blood of chronic obstructive

pulmonary disease indicate involvement of autoimmunity mechanisms. *Adv Respir Med*. 2019;87(3):159–166.
48. Cosio MG, Majo J, Cosio MG. Inflammation of the airways and lung parenchyma in COPD:role of T cells. *Chest*. 2002;121(5 Suppl):160S–165S.
49. Freeman CM, Martinez CH, Todt JC, et al. Acute exacerbations of chronic obstructive pulmonary disease are associated with decreased $CD4^+$ & $CD8^+$ T cells and increased growth & differentiation factor-15 (GDF-15) in peripheral blood. *Respir Res*. 2015;16(1):94.